doi:10.1007/s11589-010-0781-z

# Rapid afterslip and short-term viscoelastic relaxation following the 2008 $M_W$7.9 Wenchuan earthquake*

Zhigang Shao[1] Rongjiang Wang[2,♠]
Yanqiang Wu[1] and Langping Zhang[1]

[1] *Institute of Earthquake Science, China Earthquake Administration, Beijing* 100036, *China*
[2] *GFZ German Research Center for Geosciences, D*-14473 *Potsdam, Germany*

**Abstract** Significant postseismic deformation of the 2008 $M_W$7.9 Wenchuan earthquake has been observed from GPS data of the first 14 days after the earthquake. The possible mechanisms for the rapid postseismic deformation are assumed to be afterslip on the earthquake rupture plane and viscoelastic relaxation of coseismiclly stress change in the lower crust or upper mantle. We firstly use the constrained least squares method to find an afterslip model which can fit the GPS data best. The afterslip model can explain near-field data very well but shows considerable discrepancies in fitting far-field data. To estimate the effect due to the viscoelastic relaxation in the lower crust, we then ignore the contribution from the afterslip and attempt to invert the viscosity structure beneath the Longmenshan fault where the Wenchuan earthquake occurred from the postseismic deformation data. For this purpose, we use a viscoelastic model with a 2D geometry based on the geological and seismological observations and the coseismic slip distribution derived from the coseismic GPS and InSAR data. By means of a grid search we find that the optimum viscosity is $9\times10^{18}$ Pa·s for the middle-lower crust in the Chengdu Basin, $4\times10^{17}$ Pa·s for the middle-lower crust in the Chuanxi Plateau and $7\times10^{17}$ Pa·s for the low velocity zone in the Chuanxi plateau. The viscoelastic model explains the postseismic deformation observed in the far-field satisfactorily, but it is considerably worse than the afterslip model in fitting the near-fault data. It suggests therefore a hybrid model including both afterslip and relaxation effects. Since the viscoelastic model produces mainly the far-field surface deformation and has fewer degree of freedoms (three viscosity parameters) than the afterslip model with a huge number of source parameters, we fix the viscositiy structure as obtained before but redetermine the afterslip distribution using the residual data from the viscoelastic modeling. The redetermined afterslip distribution becomes physically more reasonable; it is more localized and exhibits a pattern spatially complementary with the coseismic rupture distribution. We conclude that the aseismic fault slip is responsible for the near-fault postseismic deformation, whereas the viscoelastic stress relaxation might be the major cause for the far-field postseismic deformation.

**Key words**: **Wenchuan earthquake; short-term postseismic deformation; aseismic slip; viscoelastic relaxation**
**CLC number**: P315.72$^+$5 **Document code**: A

## 1 Introduction

The $M_W$7.9 Wenchuan earthquake occurred on May 12, 2008 in Sichuan, China. Field investigation indicates that the earthquake led to the surface ruptures of two NW trending imbricate reverse faults (Beichuan-Yingxiu fault and Guanxian-Jiangyou fault) along Longmenshan nappe tectonic belt simultaneously. As shown in Figure 1, the surface rupture along the Beichuan-Yingxiu fault is about 240 km long and is a reverse fault with a significant right-lateral strike-slip component. The surface rupture along the Guanxian-

* **Received** 8 Dctober 2010; **accepted in revised form** 18 February 2011; **published** 10 April 2011.
♠ **Corresponding author. e-mail**: wang@gfz-potsdam.de

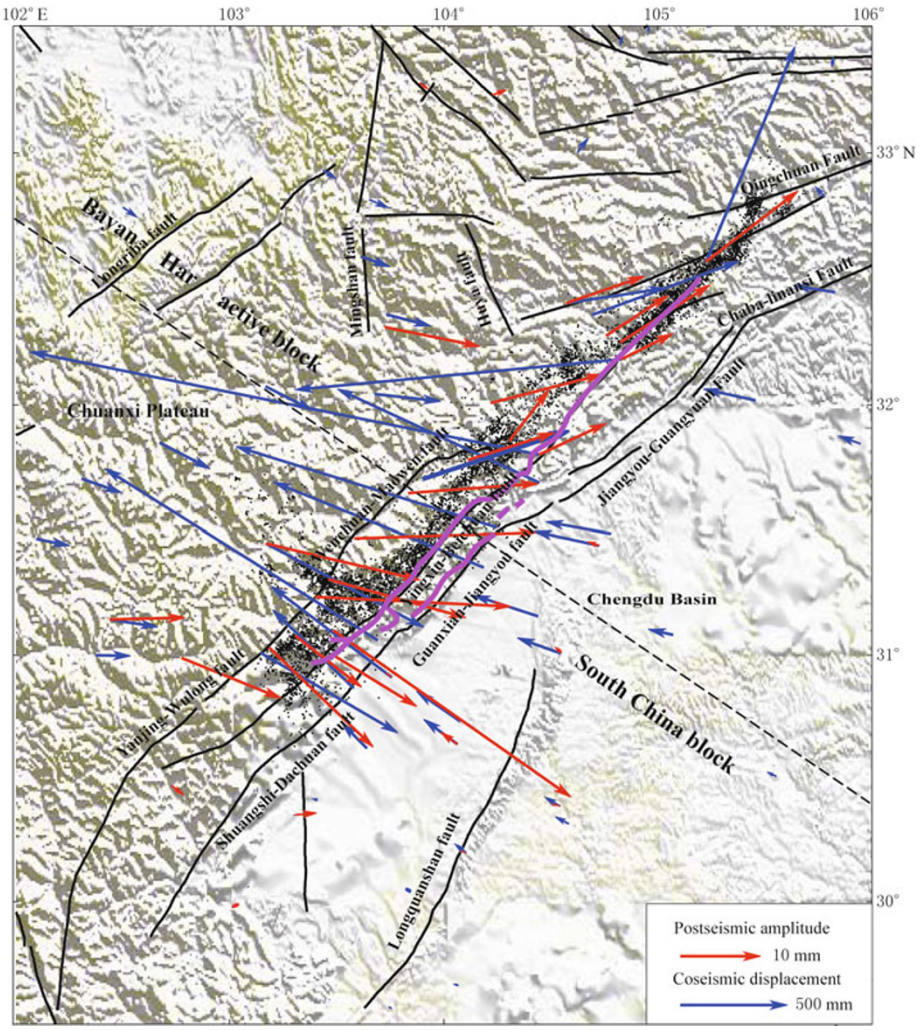


**Figure 1** Coseismic surface rupture distribution and surface displacements observed by GPS in coseismic (blue arrows) and postseismic period (red arrows) of the $M_W$7.9 Wenchuan earthquake; the pink lines represent coseismic surface rupture distribution, and the black lines denote active faults, the dashed line indicates the cross-section across the Longmenshan fault zone in Figure 2.

Jiangyou fault extends about 90 km with a continuous segment of about 72 km. The Guanxian-Jiangyou fault is dominantly a reverse fault (Xu et al., 2009).

Due to the strong intruding of the Indian Ocean plate to the Eurasian plate, the Tibetan Plateau is experiencing a strong uplifting movement. At the same time, all blocks of the Tibetan Plateau produce horizontal extrusion movements in the east and south-east directions (Tapponnier et al., 1982; Zhang et al., 2004). Confronted by high strength blocks including the Ordos Basin in the North China block and the Sichuan Basin in the South China block, the horizontal extrusion of the Tibetan Plateau produced a local thrust-nappe tectonic belt along its eastern margin, including the Longmenshan nappe tectonic belt that is boundary of blocks between the Bayan Har active block and the South China active block. The Bayan Har block belongs to one of the secondary blocks of the Tibetan Plateau. The material in the deep crust and upper mantle of the Bayan Har block moves southeastward as it is driven by the Indian Ocean Plate, but the movement is blocked by the relative strong Sichuan Basin in the Longmenshan fault. Under the continuous action as long as thousands of years and due to the interseismic block effect, the upper crust on the east side of the Bayan Har block undergoes lateral shortening deformation and right-lateral shear deformation parallel to the fault (Zhang et al., 2008; Teng et al., 2008; Wen et al., 2009).

Du et al. (2009) and Zhang et al. (2008) presented a regional geodynamic model of the Wenchuan earth-

quake based on the comprehensive geological, geophysical and geodetic observations (see Figure 2). The low velocity zone in the Bayan Har block crust stretches southeastward and terminates at the Longmenshan fault, which makes the horizontal southeast movement of the upper crust transformed to the thrust movement of the Longmenshan fault near the termination of this low velocity zone. Since the Longmenshan fault is located in the brittle layer, its rupture movement should be characterized by intermittent stick-slip movement accompanied by strong earthquake rather than long-term continuous slow displacements. During the interseismic period between two strong earthquakes, Longmenshan fault restrains the horizontal movement of upper crust of the Bayan Har block. Consequently, the displacement velocity in the decoupling zone (or low velocity zone) is much slower when it gets closer to the blocked fault zone. At the same time, the upper crust of the Bayan Har block in this decoupling zone undergoes lateral shortening deformation in direction perpendicular to the Longmenshan fault.

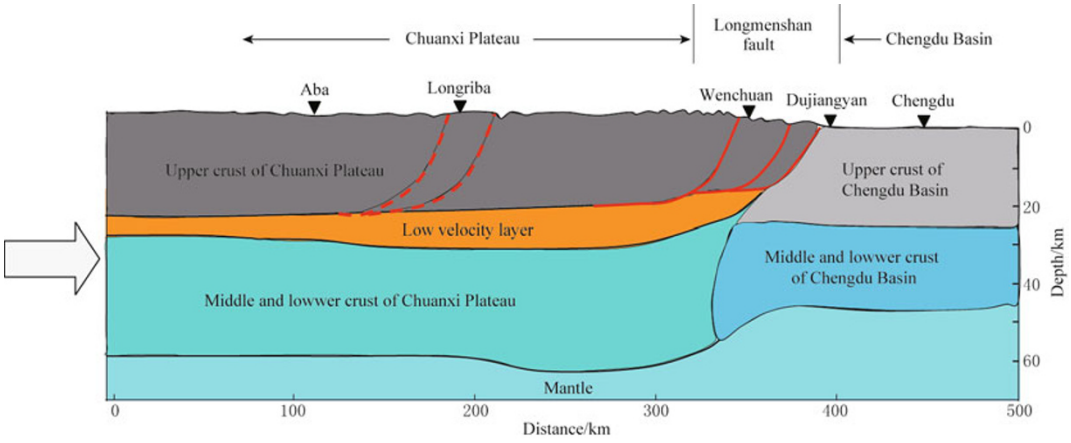


**Figure 2** Vertical profile of regional geological structure of the Longmenshan fault zone (Du et al., 2009).

## 2 Data

### 2.1 Data measured after the Wenchuan earthquake

In the frame work of two large national research projects, "Crustal Movement Observation Network of China (National Key Scientific Project) and "Dynamic Process and Strong Earthquake Prediction of Active Boundary Zone (National Programs for Fundamental Research and Development), Chinese scientists deployed a GPS network covering both sides of Longmenshan fault zone (CMONOC, 2008). It provides the coseismic displacement data of the $M_W$7.9 Wenchuan earthquake, which include 158 horizontal displacements and 46 vertical displacements (Xu et al., 2010; Hao et al., 2009). In addition, various seismic waveform data (Wang et al., 2008) and static ground deformation data derived from the near-field strong motion records (Shao et al., 2010b) are available, too. All these data provide good constraints on the coseismic fault slip of the $M_W$7.9 Wenchuan earthquake.

After Wenchuan earthquake, the Japan Aerospace Exploration Agency (JAXA) arranged a mission of emergency and obtained a batch of high precision L-band SAR data (ALOS/PALSAR), in which six adjacent ascending tracks (tracks 471, 472, 473, 474, 475, and 476) covered the whole surface rupture zone of the earthquake. Xu et al. (2010) used arc-second SRTM DEM dataset to remove the topography contibution, SNAPHU software to unwrap the differential interferograms and GAMMA software to process the range change offsets.

Based on the postseismic GPS observations, Shen et al. (2009) derived the equivalent accumulated displacements within 14 days after the earthquake. Three possible mechamisms can interpret the short-term postseismic deformation: (1) aseismic slip (also called afterslip) on the earthquake fault, (2) viscoelastic relaxation and (3) poroelatic rebound. The aseismic slip after an earthquake occurred on the coseismic rupture fault, in the sediments above the fault or in the creep layer below the fault (Marone et al., 1991; Scholz et al., 1969). The postseismic viscoelastic relaxation effect refers to crustal deformation caused by postseismic de-

layed response of middle-lower crust or rheological layer in the mantle (Nur and Mavko 1974; Deng et al., 1998). The postseismic poroelastic rebound effect refers to crustal deformation resulting from local fluid adjustment of the sediment layer in seismogenic zone (Jonsson et al., 2003). Surface deformation caused by the poroelastic rebound effect is generally characterized by movements in the vertical direction. However, the observed postseismic deformation of the Wenchuan earthquake is dominated in the horizontal direction. Therefore, in this study we attempt to model the short-term postseismic deformation data using the afterslip and viscoelastic relaxation mechanisms separately as well as jointly.

### 2.2 Regional geological model

Seismic profiles across the western Sichuan Basin, Longmenshan and Bayan Har block indicate a drastic change of crust thickness across the Longmenshan fault. A low velocity layer (high-conductivity layer) has also been found at depth of 25–30 km, which is first gently dipping to northwest in the Longmenshan fault and then gradually extends horizontally in the northwestern Bayan Har block (Wang et al., 2003; Zhu, 2008; Teng et al., 2008). The southeast end of this low velocity layer terminates beneath the place located between the Longmenshan fault. Below the low-velocity layer are middle- and lower- crust with relatively higher velocity and harder material. The velocity structures of the crust and mantle on both sides of the Longmenshan fault used in this study are obtained by previous geophysical observations and shown in Table 1.

The Young modulus can be approximately expressed by the seismic P wave velocity,

$$E = \frac{2}{3}(1+\upsilon)\rho v_{\mathrm{P}}^2. \quad (1)$$

The top of the low velocity layer is close to the depth of lower limit of aftershock distribution of the Wenchuan earthquake (Huang et al., 2008). Therefore, the depth of 25 km is regarded as the interface between viscoelastic and elastic medium. Deng et al. (1998) and Sheu and Shieh (2004) argued that the postseismic viscoelastic relaxation of the crust-mantle is mainly due to the viscoelastic relaxation of the middle and lower crust. So the upper crust is considered as elastic and the viscosity of the mantle is much larger than that in the middle and lower crust.

## 3 Modeling of the coseismic and short-term postseismic deformation

### 3.1 Coseismic displacements

Based on the existing coseismic dislocation models of the $M_{\mathrm{W}}$7.9 Wenchuan earthquake, Xu et al. (2010) divided the fault into two major parts, the Beichuan-Yingxiu fault and the Guanxian-Jiangyou fault considering both coseismic rupture and regional geological structure. The Beichuan-Yingxiu fault can be further divided into the Hongkou-Yuejiashan fault and the Beichuan-Qingchuan fault. Therefore, the coseismic rupture of the earthquake can be divided into five subfaults: the Qingchuan, Beichuan, Yuejiashan, Hongkou and Hanwang sub-faults, numbered from 1 to 5, respectively. The end dip angle of all five sub-faults in depth is uniformly set to 20°. The start dip angles of the five sub-faults on the surface are 60°, 46°, 60°, 42° and 44° respectively. The dip angles transform from the surface to the depth of 24 km, approaching to the top of the low velocity layer of Chuanxi Plateau. The 3D view of the sub-faults is shown in Figure 3.

Table 1 Seismic reference model of both sides of the Longmenshan fault zone (Zhu, 2008)

| Model | Layer | Thickness/km | $v_{\mathrm{P}}$/km·s$^{-1}$ | $v_{\mathrm{S}}$/km·s$^{-1}$ | $\rho$/kg·m$^{-3}$ | $\nu$ | $E/10^{11}$ Pa |
|---|---|---|---|---|---|---|---|
| Tibetan Plateau | 1 | 5 | 5.20 | 3.00 | 250 0 | 0.25 | 0.56 |
| | 2 | 10 | 6.10 | 3.52 | 280 0 | 0.25 | 0.87 |
| | 3 | 10 | 6.20 | 3.58 | 285 0 | 0.25 | 0.91 |
| | 4 | 5 | 6.00 | 3.46 | 275 0 | 0.25 | 0.82 |
| | 5 | 15 | 6.70 | 3.87 | 295 0 | 0.25 | 1.10 |
| | 6 | 15 | 7.40 | 4.27 | 310 0 | 0.25 | 1.41 |
| Chengdu Basin | 7 | 10 | 5.20 | 3.00 | 250 0 | 0.25 | 0.56 |
| | 8 | 5 | 6.00 | 3.46 | 275 0 | 0.25 | 0.83 |
| | 9 | 5 | 6.30 | 3.64 | 285 0 | 0.25 | 0.94 |
| | 10 | 15 | 6.70 | 3.87 | 295 0 | 0.25 | 1.10 |
| | 11 | 10 | 7.40 | 4.27 | 310 0 | 0.25 | 1.41 |
| Mantle | 12 | – | 8.00 | 4.62 | 340 0 | 0.25 | 1.81 |

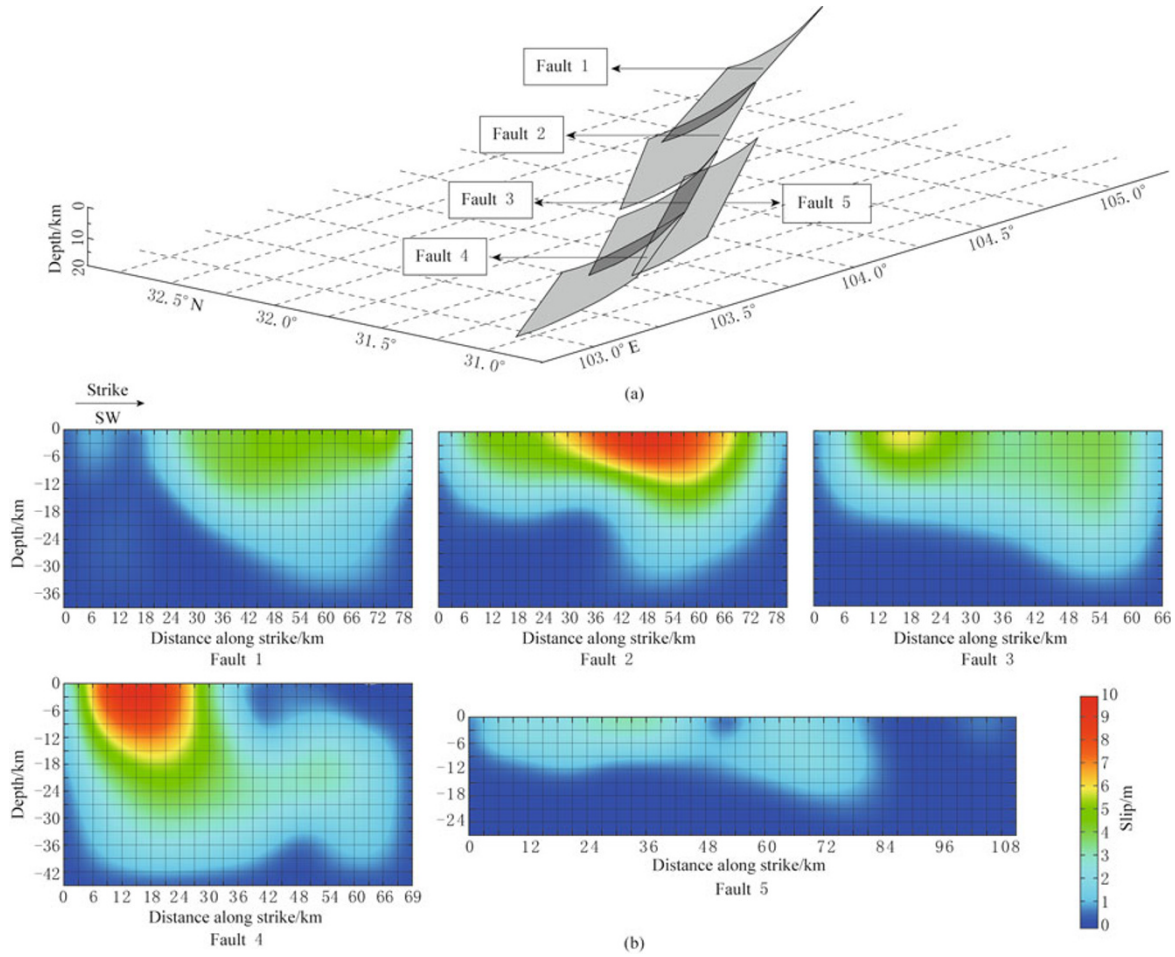


**Figure 3** 3D fault model of the $M_W$7.9 Wenchuan earthquake (a). Coseismic slip distribution derived from the joint inversion of GPS, InSAR and strong motion data (b).

Using the constrained least squares method (Diao et al., 2010), Xu et al. (2010) derived the coseismic slip distribution of the five sub-faults. The data they used include the 158 horizontal and 46 vertical GPS displacements as mentioned above and 3 801 re-sampled InSAR LOS displacements derived from six high precision L-band SAR (PALSAR) data (Hashimoto et al., 2009). To better estimate the coseismically induced stress change distribution, we update the slip model by Xu et al. (2010) by including additional static surface displacement data derived from the 43 near-field strong motion records via the baseline correction (Shao et al., 2010b). This data set will be called hereafter simply SM data.

The updated slip distribution from joint inversion of all GPS, InSAR and SM data is shown in Figure 3b. The whole slip pattern differs only slightly from that given by Xu et al. (2010), implying that the SM data are well consistent with the GPS and InSAR data. The slip on the Beichuan and Hongkou sub-faults are larger

Table 2 Fault parameters of the 2008 $M_W$7.9 Wenchuan earthquake

| No. of fault | Sub-fault | Reference latitude/°N | Reference longitude/°E | Length /km | Width /km | Strike /° | Dip angles | |
|---|---|---|---|---|---|---|---|---|
| | | | | | | | Start | End |
| 1 | Qingchuan | 32.64 | 105.45 | 81 | 39 | 228.8 | 60° | 20° |
| 2 | Beichuan | 32.16 | 104.80 | 81 | 39 | 221.1 | 46° | 20° |
| 3 | Yuejiashan | 31.61 | 104.17 | 66 | 39 | 223.9 | 60° | 20° |
| 4 | Hongkou | 31.18 | 103.73 | 72 | 45 | 227.1 | 42° | 20° |
| 5 | Hanwang | 31.63 | 104.37 | 111 | 27 | 228.4 | 44° | 20° |

Note: All sub-faults have a listric form with dip angle linearly decreasing from the surface to depth. The reference point of each sub-fault is its northeast upper corner. The width refers to the width of sub-fault along dip.

than that on the other sub-faults. The maximum slips on both the sub-faults are close to 10 m. The equivalent moment magnitude is $M_{\rm W}$7.9 in good agreement with the teleseismic observation.

### 3.2 Afterslip model

As the same as the coseismic slip, we use the same linear inversion method to derive the postseismic afterslip of the Wenchuan earthquake from GPS data of the first 14 days (Figure 4a). The result is shown in Figure 4b. The magnitude of this short-term afterslip corresponds to $M_{\rm W}$6.8. Significant afterslips are found on the Hongkou and Hanwang sub-faults both with peak value of about 10 cm. Except for the Hanwang sub-fault, the afterslip distribution of the other sub-faults exhibits a pattern looking like a smooth extension of the coseismic slip distribution (Figure 3b) at depth. In particular, it looks like to be cut off artificially at the lower boundary of the fault. The reason may be attributing to fit the two far-field stations on the Tibetan Plateau with significant postseismic movements. The data fit with the afterslip model is excellent in whole, except for a few far-field stations. The correlation coefficient between the predicted and observed postseismic displacements is about 95

### 3.3 Viscoelastic model

To estimate the effect due to relaxation of the coseismic stress change in the lower crust and upper mantle, we construct three different viscoelastic models with a uniform 2D geometry based on the geological crust structure of the Longmenshan fault zone (Figure 2). The finite element method (FEM) is extensively used in modeling postseismic deformation (Deng et al., 1998; Masterlark, 2000; Freed and Brgmann, 2004). We use the software named Finite Element Program Generator to obtain different Fortran FEM programs based on different equations (Shao et al., 2010a). An irregular 59×49×25 3D finite element grids covering 910, 802, 270 km in the northeast, southeast and vertical directions, respectively which was used to simulate the time-dependent displacement based on Maxwell model.

Following Deng et al. (1998), we set the mantle viscosity to be $1.0\times10^{20}$ Pa·s. In model $A$ (Figure 5b), the low velocity layer below the Chuanxi Plateau is regarded as elastic. In model $B$ (Figure 5c), the low velocity layer is regarded as viscoelastic with the same viscosity as the lower crust of the Chuanxi Plateau. Then various finite element modeling (FEM) procedures are carried out to find the optimum viscosity values used in models $A$ and $B$ that best fit the GPS data. To evaluate the misfit of the models to the observation, we use the formula by Lorenzo et al. (2006),

$$\Delta=\sum_{i=1}^{32}\left[\left(\frac{x_i-x_i^{\rm GPS}}{\sigma_{x_i}}\right)^2+\left(\frac{y_i-y_i^{\rm GPS}}{\sigma_{y_i}}\right)^2\right] \quad (2)$$

where $(x_i^{\rm GPS},\ y_i^{\rm GPS})$ are the NS and EW components of the surface displacement observed at the i*th* GPS station, $(x_i,\ y_i)$ are the corresponding modeling results, and $(\sigma_{x_i},\ \sigma_{y_i})$ are the corresponding observation errors. Model $C$ (Figure 5d) adopts the viscosity structure of model $B$ except for the low velocity layer, which is optimized separately.

To optimize the viscosities of the lower crust in the Chengdu Basin and in the Chuanxi Plateau, a 2D grid search approach is used. Figures 6a and 6b show the results with 784 FEM modeling running for models $A$ and $B$, respectively. In both cases, the viscosity of the lower crust in the Chuanxi Plateau is considerably better constrained than that in the Sichuan Basin. In both models $A$ and $B$, the optimum viscosity of the lower crust in the Chuanxi Plateau is about $4\times10^{17}$ Pa·s that is about one order smaller than the optimum viscosity of the lower crust in the Chengdu Basin. The latter is roughly $5\times10^{18}$ Pa·s in model $A$ and $9\times10^{18}$ Pa·s in model $B$. In model $C$, the viscosity of the low velocity layer beneath the Chuanxi Plateau is optimized by fixing the viscosities of the lower crust in the Chengdu Basin and in the Chuanxi Plateau as determined in model $B$. The optimum viscosity of the low velocity layer is about $7\times10^{17}$ Pa·s (Figure 6c), a little bit larger than the lower crust below it. Figure 7 shows the comparison between the surface displacements within 14 days after earthquake observed by GPS and that predicted using model $C$. The viscoelastic model explains the postseismic deformation observed in the far field satisfactorily, but it is considerably worse than the afterslip model in fitting the near-fault data.

### 3.4 The hybrid model

It is assumed that the afterslip mainly occurs at the coseismic rupture plane within the seismogenic zone, whereas the viscoelastic relaxation occurs in the lower crust and upper mantle below the seismogenic zone. The hybrid model will include the two different effects. Since the viscoelastic model produces mainly the far-field surface deformation and has much less freedom (three viscosity parameters) than the afterslip model with a huge number of source patches, we fix the viscosity structure as obtained before but invert the afterslip distribution from the residual data (the residual postseismic GPS displacements after subtracting the viscoelastic relaxation effect) by the viscoelastic modeling (Figure 8a).

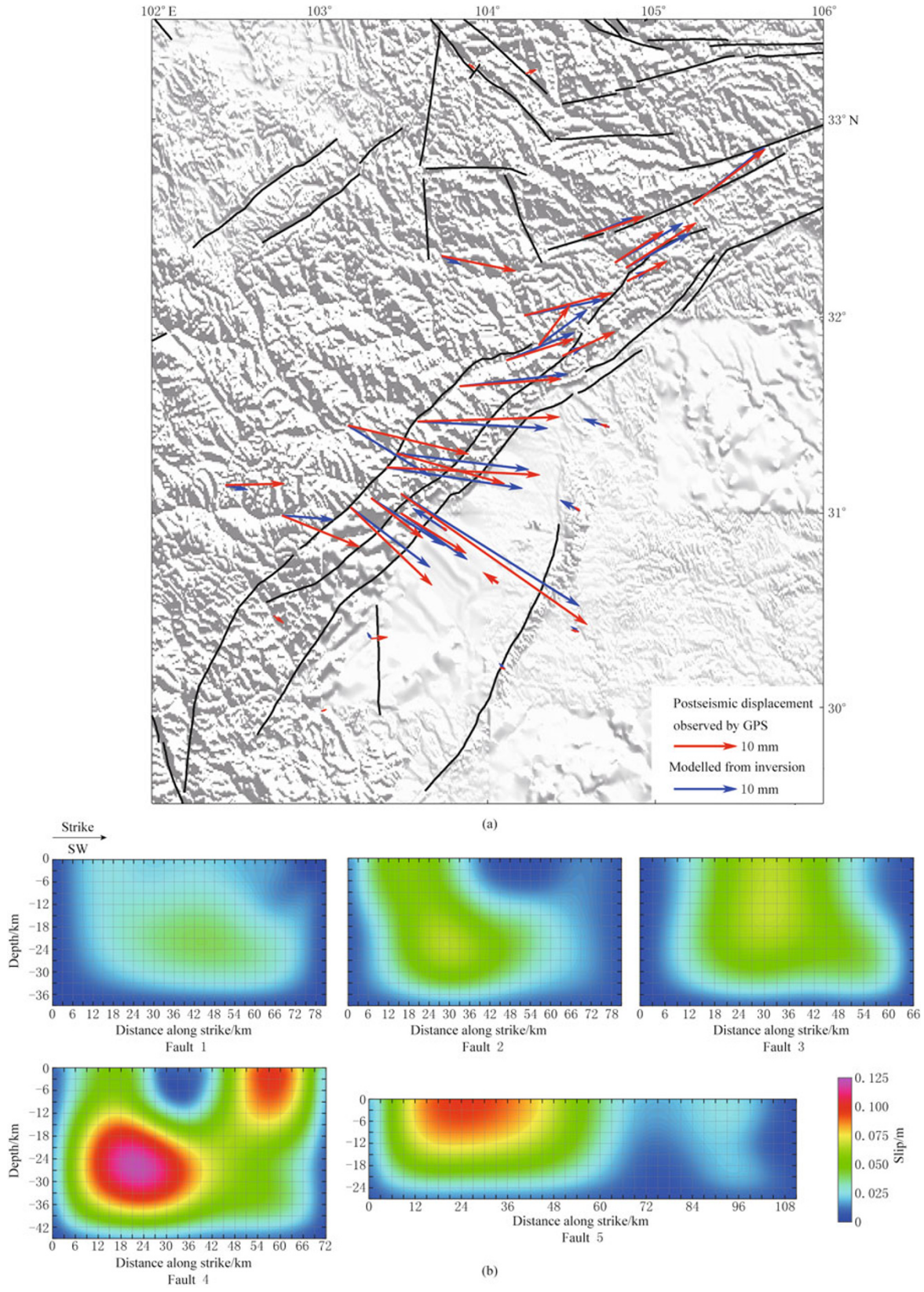


**Figure 4** The inversion result of postseismic afterslip. (a) Comparison between the observed and predicted horizontal surface displacements in the first 14 days after the Wenchuan earthquake. (b) Afterslip distribution on the coseismic sub-faults 1–5 inverted from the first 14 days of GPS data.

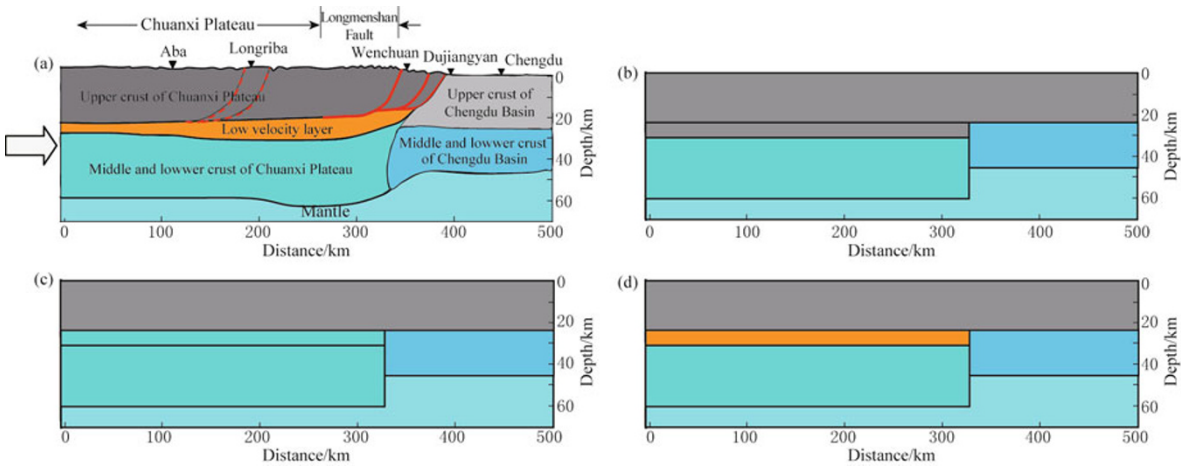


**Figure 5** Viscoelastic models based on the geological structure of the Longmenshan fault zone. (a) is the same as the Figure 2. (b–d) Viscoelastic models $A$, $B$ and $C$, respectively. The grey color denotes elastic blocks and other colors denote viscoelastic blocks with different viscosities.

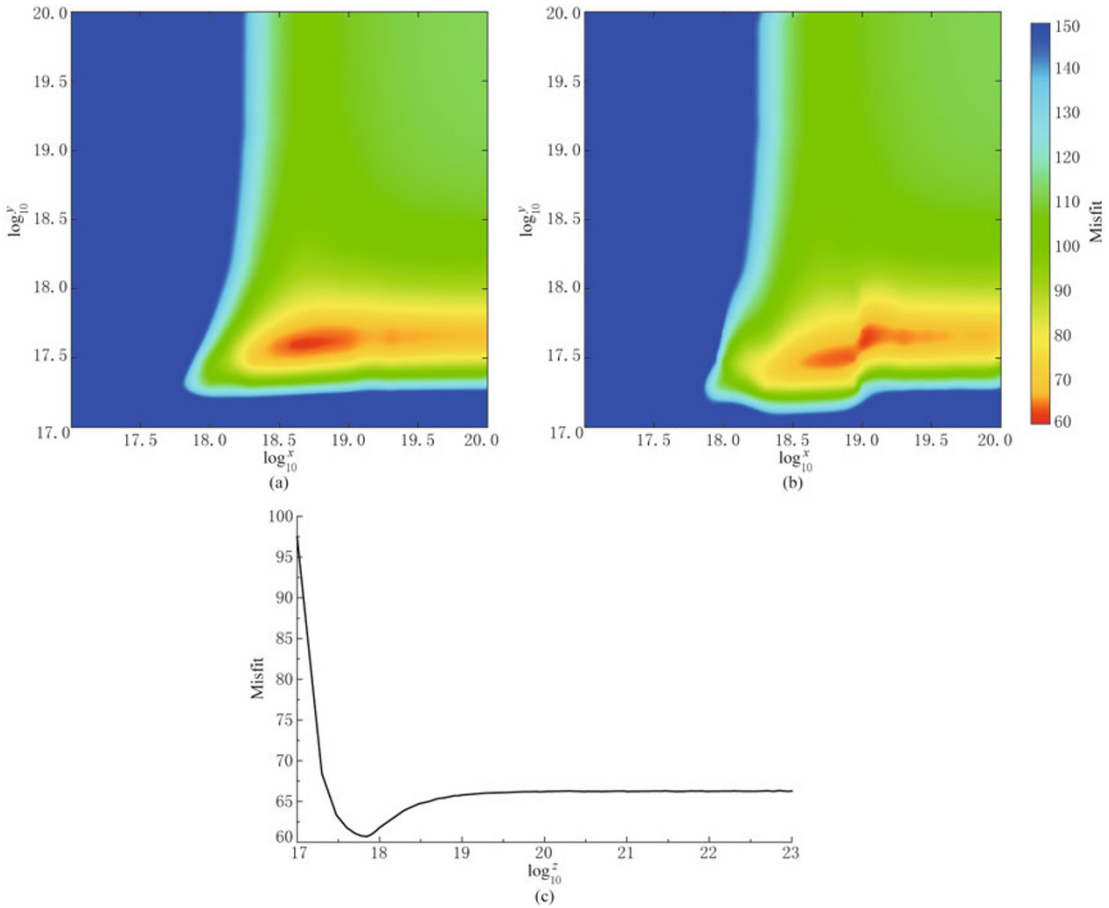


**Figure 6** Misfit calculated by equation (2) between the predicted and observed postseismic surface displacements depending on the viscosity structures used. (a) Model $A$ (the optimum viscosity of the lower crust in the Chengdu Basin and in the Chuanxi Plateau are $5\times10^{18}$ Pa·s and $4\times10^{17}$ Pa·s, respectively). (b) Model $B$ (the optimum viscosity of the lower crust in the Chengdu basin and in the Chuanxi plateau are $9\times10^{18}$ Pa·s and $4\times10^{17}$ Pa·s, respectively). In Figures 6a and 6b, $x$ refers to viscosity of lower crust in Chengdu Basin and $y$ stands for viscosity of lower crust in Chuanxi Plateau. (c) Model $C$ (the optimum viscosity of the low velocity layer is $7\times10^{17}$ Pa·s), $z$ refers to viscosity of low velosity layer.

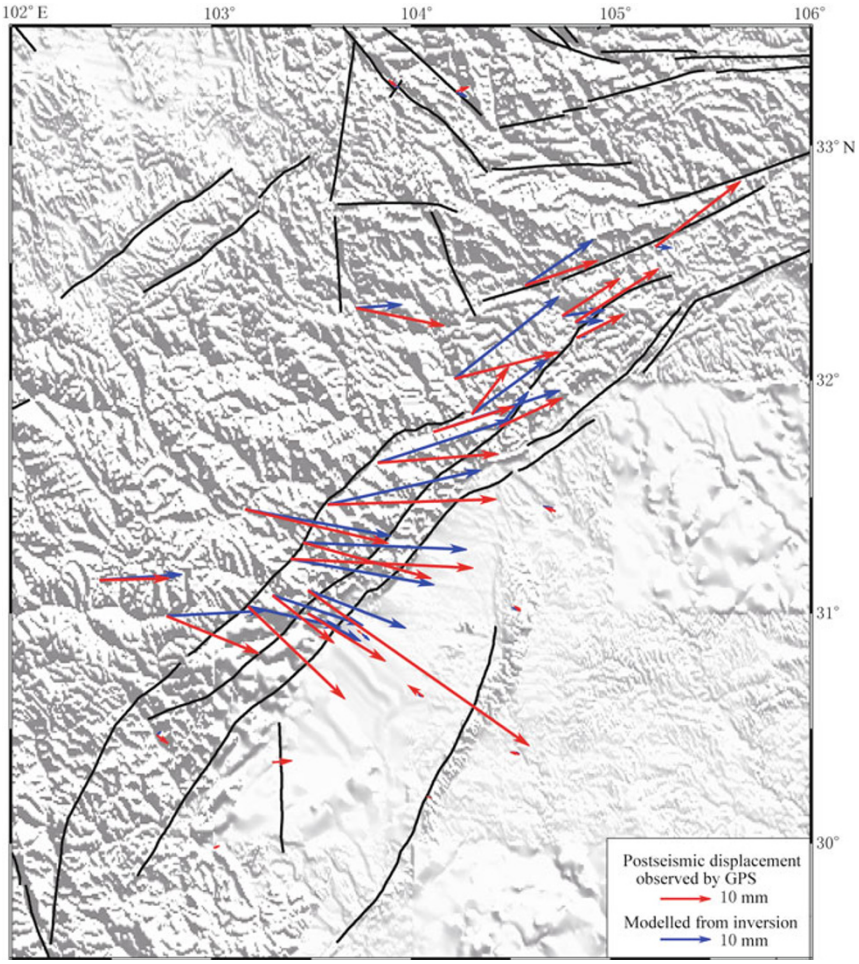


**Figure 7** Comparison between the surface displacements observed by GPS within 14 days after earthquake (red arrows) and that calculated by FEM simulation using the optimum viscoelastic relaxation model (blue arrows).

The afterslip distribution obtained in this way is shown in Figure 8c. Its magnitude is $M_W$6.4, significantly smaller than $M_W$6.8 as obtained by the separate inversion without the correction for the relaxation effect. In the Yingxiu-Beichuan and Hanwang sub-faults, the afterslips are apparently complementary in space with and the coseismic rupture (Figure 3b). Except for the Yuejiashan sub-fault where the afterslip is insignificant, all other sub-faults include one or two localized afterslip clusters larger than 4 cm. In particular, no artificial cut-off of the afterslip at the lower margin of the fault plane is visible.

## 4 Discussion and conclusions

We calculate the correlation coefficients between the short-term postseismic surface displacements simulated by different models and those observed by the GPS using the formula by Sheu et al. (2004),

$$r = \frac{N\sum_{i=1}^{N} x_i y_i - \sum_{i=1}^{N} x_i \sum_{i=1}^{N} y_i}{\left[N\sum_{i=1}^{N} x_i^2 - \left(\sum_{i=1}^{N} x_i\right)^2\right]^{1/2}\left[N\sum_{i=1}^{N} y_i^2 - \left(\sum_{i=1}^{N} y_i\right)^2\right]^{1/2}} \quad (3)$$

where $x_i$ and $y_i$ are the observed and simulated displacement components, respectively, and $N$ is the number of data. The results are shown in Figure 9.

Generally, the agreement between two groups of data is regarded as good if their correlation coefficient is greater than 0.7. For the coseismic surface displacements in the east-west and south-north directions, the correlation coefficients between the observation and the dislocation model are 0.99 and 0.92, respectively,

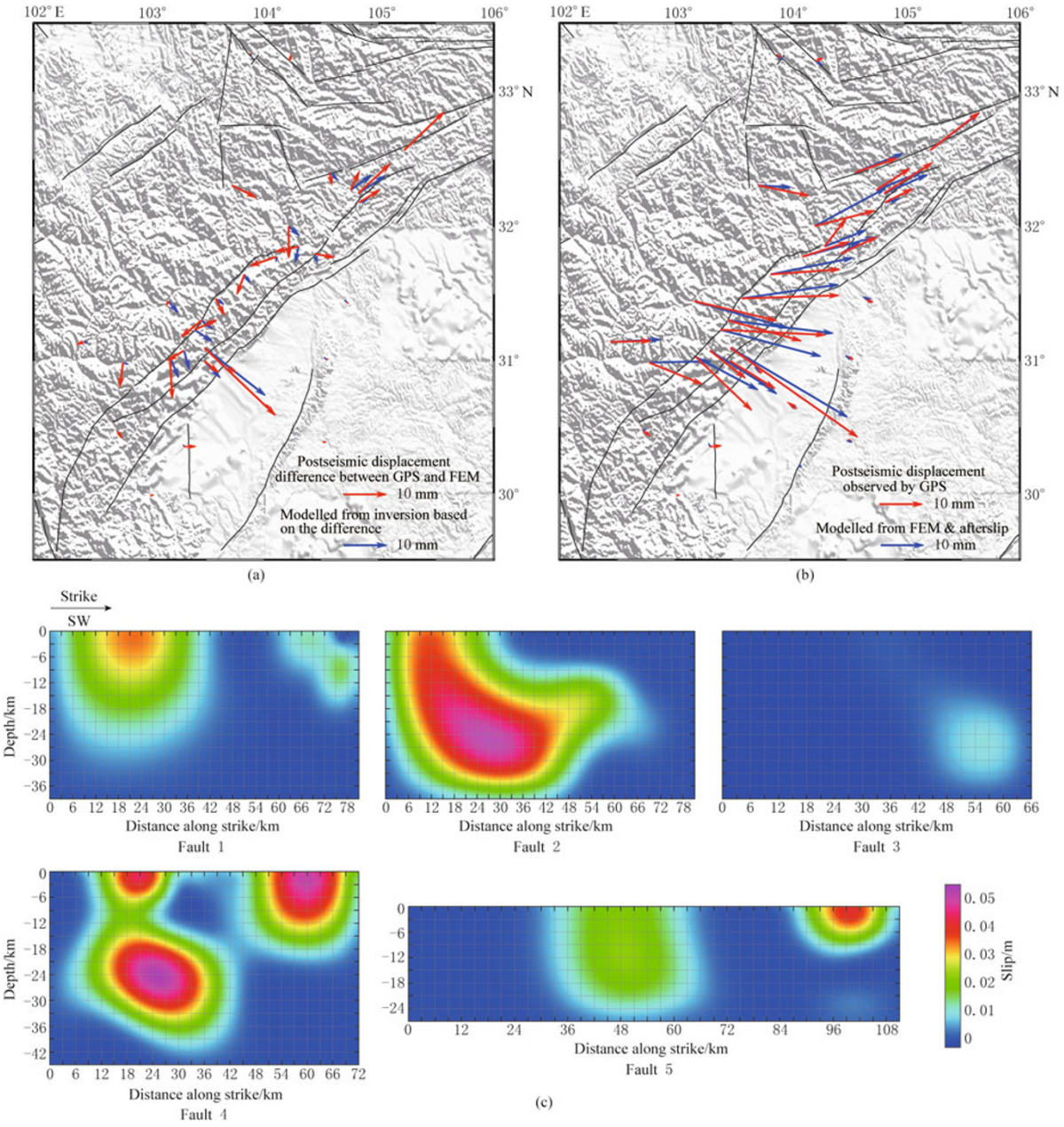


**Figure 8** Comparison between the residual postseismic GPS displacements after subtracting the viscoelastic relaxation effect (red arrows) and the displacements calculated for the best-fit afterslip model shown in (c) (blue arrows). (b) Comparison between the total postseismic GPS displacements (red arrows) and the displacements calculated for the hybrid model with both relaxation and afterslip effects (blue arrows). (c) Afterslip distribution inverted from the residual postseismic GPS displacements after subtracting the viscoelastic relaxation effect.

showing that the joint inversion using the GPS, InSAR and SM data is highly reliable (Figure 9a).

The GPS stations with relatively large postseismic displacements are mostly located near the coseismic rupture trace of the earthquake. Assuming that the postseismic deformation is caused solely by afterslips at the coseismic fault plane, the correlation coefficient between the data and the best-fit afterslip model is 0.94 for the east-west component and 0.95 for the north-south component (Figure 9b). Especially the afterslip model can reproduce the near-field data better than the far-field data.

When assuming that the postseismic deformation is caused solely by the relaxation of the coseismically induced stress changes in the lower crust and upper mantle, the correlation coefficient between the data

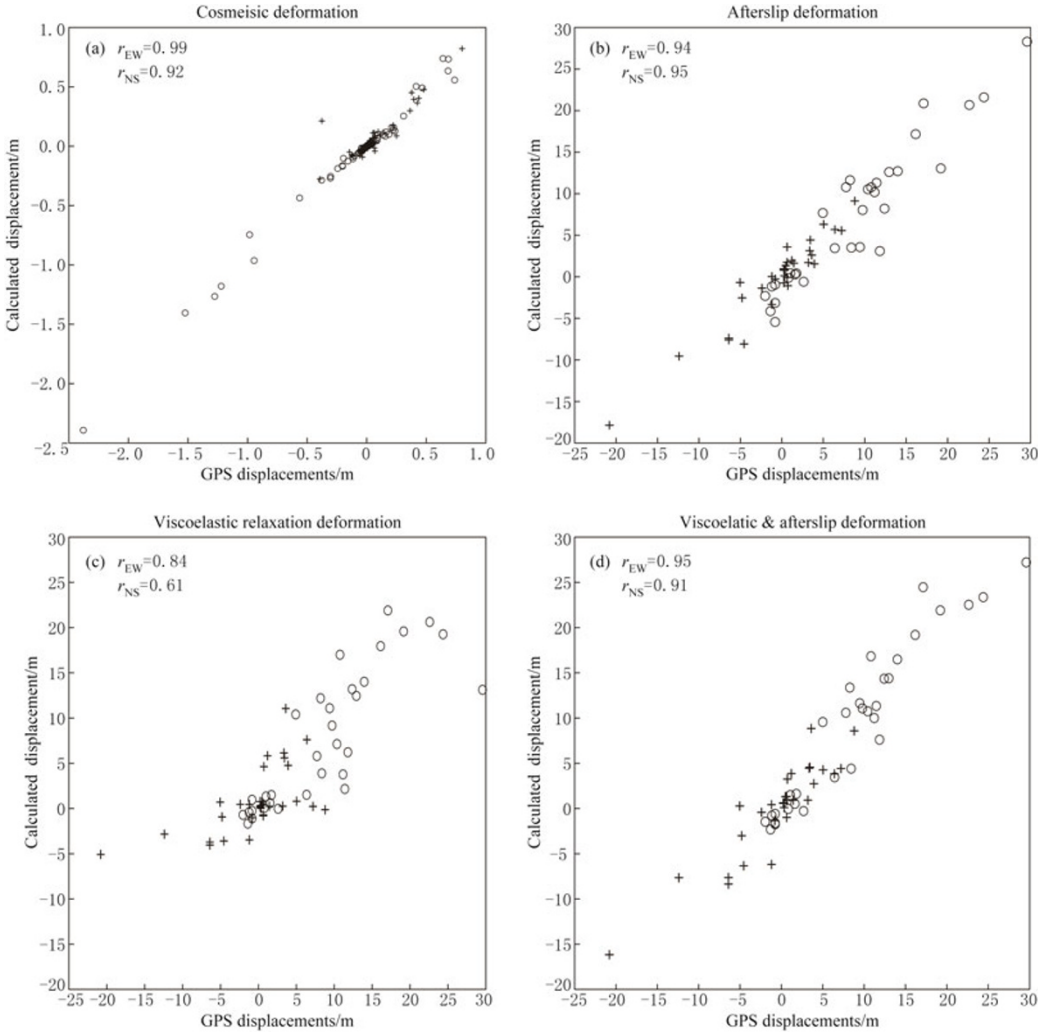


**Figure 9** Comparison between the observed co- and postseismic deformation of the 2008 $M_W$7.9 Wenchuan earthquake with the corresponding predictions based different assumptions on the deformation mechanisms. The south-north component is represented by cross and the east-west component by circle. The correlation coefficients between the data and model for both components are shown on top of each panel. (a) The observed coseismic GPS displacements versus the corresponding predictions calculated from the coseismic slip model derived from the GPS, InSAR and SM data by joint inversion. (b–d) The observed postseismic GPS displacements versus the corresponding predictions calculated for the pure afterslip (b), the pure viscoelastic relaxation model (c) and the hybrid model (d), respectively.

and model becomes 0.84 for the east-west component and 0.61 for the north-south component (Figure 9c). Particularly, the viscoelastic relaxation model can reproduce the displacements observed at the far-field GPS stations better than the afterslip model. From the statistic point of view, it can be concluded that the observed short-term postseismic deformation may include certain contribution from the viscoelastic relaxation effect. Moreover, it yields that the best-fit viscosity of the lower crust in the Sichuan Basin is at least one order larger than that in the Chuanxi Plateau, which is consistent with the tectonic movement observed in the Longmenshan region.

The hybrid model includes both afterslip and relaxation effects. For simplicity, the afterslip distribution and the viscosity structure of the hybrid model are not determined jointly but successively, i.e., the afterslip distribution in the hybrid model is derived from the residual data after subtracting the relaxation effect. The correlation coefficient between the data and the hybrid model is 0.95 for the east-west component and 0.91 for the north-south component (Figure 9d). The cause

for the slightly smaller correlation coefficients than the pure afterslip model is probably the over-estimate of the viscoelastic relaxation effect due to the non-joint inversion. However, it can be seen from comparison between Figure 4b and Figure 8c that the afterslip distribution of the hybrid model is more localized and exhibits a pattern spatially complimentary with the coseismic rupture distribution. This feature of the afterslip is physically more reasonable, since there is generally large deficit of the stress release around the coseismic slip asperities.

We conclude that the aseismic fault slip is responsible for the near-fault postseismic deformation, whereas the viscoelastic stress relaxation might be the major cause for the far-field postseismic deformation. The data fit of the hybrid model can be improved using the joint inversion approach, but with considerably larger computation effort.

**Acknowledgements** We thank Prof. Zaisen Jiang and Prof. Guomin Zhang for helpful discussion and Dr. Youyi Ruan for proofread of this manuscript. This work was supported by the Basic Research Foundation of Institute of Earthquake Science, China Earthquake Administration (02092421).

## References

The Crustal Movement Observation Network of China (CMONOC) 2008. Coseismic signals of the 2008 $M_S$8.0 Wenchuan earthquake determined with GPS. *Science in China* (*Series D*) **38**(10): 1 195–1 206 (in Chinese).

Deng J, Gurnis M, Kanamori H and Hauksson (1998). Viscoelastic flow in the lower crust after the 1992 Landers, California, earthquake. *Science* **282**: 1 689–1 692.

Diao F, Xiong X, Wang R, Zhang Y and Hsu H (2010). Slip model of the 2008 $M_W$7.9 Wenchuan (China) earthquake derived from coseismic GPS data. *Earth Planets Space* doi:10.5047/eps.2009.05.003.

Du F, Wen X Z, Zhang P Z and Wang Q L (2009). Interseismic deformation across the Longmenshan fault zone before the $M_S$8.0 Wenchuan earthquake. *Chinese J Geophys* **52**(11): 2 729–2 738 (in Chinese with English abstract).

Freed A and Bürgmann R (2004). Evidence of powerlaw flow in the Majave desert mantle. *Nature* **430**: 548–551.

Hao K X, Si H J, Fujiwara H and Ozawa T (2009). Coseismic surface-ruptures and crustal deformations of the 2008 $M_W$7.9 Wenchuan earthquake, China. *Geophys Res Lett* **36**: L11303, doi:10.1029/2009GL037971.

Hashimoto M, Enomoto M and Fukushima Y (2009). Coseismic deformation from the 2008 Wenchuan, China, earthquake derived from ALOS/PALSAR images. *Tectonophysics* doi:10.1016/j.tecto.2009.08.034.

Huang Y, Wu J P, Zhang T Z and Zhang D N (2008). Relocation of the M8.0 Wenchuan earthquake and its aftershock sequence. *Science in China* (*Series D*) **51**(12): 1 703–1 711 (in Chinese with English abstract).

Jonsson S, Segall P, Pedersen R and Bjomsson (2003). Post-earthquake ground movements correlated to porepressure transients. *Nature* **424**: 179–183.

Lorenzo M F, Roth F and Wang R (2006). Inversion for rheological parameters from post-seismic surface deformation associated with the 1960 Valdivia earthquake, Chile. *Geophys J Int* **164**: 75–87.

Marone C J, Scholz C H and Bilham R (1991). On the mechanics of earthquake afterslip. *J Geophys Res* **96**: 8 441–8 452.

Masterlark T L (2000). Regional fault mechanics following the 1992 Landers earthquake. [Ph D Dissertation]. Madison, WI, University of Wisconsin-Madison.

Nur A and Mavko G (1974). Post-seismic viscoelastic rebound. *Science* **183**: 204–206.

Scholz C H, Wyss M and Smith S W (1969). Seismic and aseismic slip on the San Andreas fault. *J Geophys Res* **74**: 2 049–2 069.

Shao Z G, Fu R S and Jiang C S (2010a). Short-time postseismic deformation of 2001 $M_S$8.1 Kunlun (China) earthquake. Concurrency Computat.: Pract. Exper., **22**: 1 803–1 812.

Shao Z G, Zhou C H, Wang R J and Zhang Y J (2010b). The basin correction of strong motion of Wenchuan $M_S$8.0 earthquake and application in the inversion of displacement. submitted.

Shen Z K, Sun J, Zhang P, Wan Y, Wang M, Bürgmann R, Zeng Y, Gan W, Liao H and Wang Q (2009). Slip maxima at fault junctions and rupturing of barriers during the 2008 Wenchuan earthquake. *Nature Geoscience* **2**: 718–724.

Sheu S and Shieh C (2004). Viscoelastic-afterslip concurrence: a possible mechanism in the early post-seismic deformation of the $M_W$7.6, 1999 Chi-Chi (Taiwan). *Geophys J Int* **159**: 1 112–1 124.

Tapponnier P, Peltzer G, Le Dain A Y, Armijo R and Cobbold P (1982). Propagating extrusion tectonics in Asia: New insights from simple experiments with plasticine. *Geology* **10**(12): 611–616.

Teng J W, Bai D H, Yang H, Yan X F, Zhang H S, Zhang Y Q and Ruan X M (2008). Deep processes and dynamic resposes associated with the Wenchuan $M_S$8.0 earthquake of 2008. *Chinese J Geophys* **51**(5): 1 385–1 102 (in Chinese with English abstract).

Wang C Y, Wu J P, Lou H, Zhou M D and Bai Z M (2003). The P wave crustal structure of West Sichuan, China. *Science in China* (*Series D*) **33**(Suppl.): 181–189 (in Chinese with English abstract).

Wang W M, Zhao L F, Li J and Yao Z X (2008). Rupture process of the $M_S$8.0 Wenchuan earthquake of Sichuan,

China. *Chinese J Geophys* **51**(5): 1 403–1 410 (in Chinese with English abstract).

Wen X Z, Zhang P Z, Du F and Long F (2009). The background of historical and modern seismic activities of the occurrence of the 2008 $M_S$8.0 Wenchuan, Sichuan, earthquake. *Chinese J Geophys* **52**(2): 444–454 (in Chinese with English abstract).

Xu C, Liu Y, Wen Y and Wang R J (2010). Coseismic slip distribution of the 2008 $M_W$7.9 Wenchuan earthquake from joint inversion of GPS and InSAR data. *Bull Seismol Soc Am* **100**: 2 736–2 749

Xu X, Wen X, Yu G Chen G, Klinger Y, Hubbard J and Shaw J (2009). Coseismic reverse- and oblique-slip surface faulting generated by the 2008 $M_W$7.9 Wenchuan earthquake, China. *Geology* **37**(6): 515–518 (in Chinese with English abstract).

Zhang P Z, Xu X W, Wen X Z and Ran Y K (2008). Slip rates and recurrence intervals of the Longmenshan active fault zone, and tectonic implications for the mechnanism of the May 12 Wenchuan earthquake, 2008, Sichuan, China. *Chinese J Geophys* **51**(4): 1 066–1 073 (in Chinese with English abstract).

Zhang P, Shen Z, Wang M, Gan W, Bürgmann R, Molnar P, Wang Q, Niu Z, Sun J, Wu J, Sun H and You X (2004). Continuous deformation of the Tibetan Plateau from Global Positioning System data. *Geology* **32**: 809–812 (in Chinese with English abstract).

Zhu J S (2008). The Wenchuan earthquake occurrence background in deep structure and dynamics of lithosphere. *Journal of Chengdu University of Technology* (*Science and Techonlogy Edition*) **35**(4): 348–356 (in Chinese with English abstract).